Society For Biomaterials

Surface topography of silicon nitride affects antimicrobial and osseointegrative properties of tibial implants in a murine model

Masahiro Ishikawa,[1] Karen L. de Mesy Bentley,[1,2,3] Bryan J. McEntire ,[4] B. Sonny Bal,[4,5] Edward M. Schwarz,[1,2,3] Chao Xie[1,3]

[1]Center for Musculoskeletal Research, University of Rochester School of Medicine and Dentistry, Rochester, New York, USA
[2]Department of Pathology and Laboratory Medicine, University of Rochester School of Medicine and Dentistry, Rochester, New York, USA
[3]Department of Orthopaedics, University of Rochester School of Medicine and Dentistry, Rochester, New York, USA
[4]Amedica Corporation, Salt Lake City, Utah, USA
[5]Department of Orthopaedic Surgery, University of Missouri, Columbia, Missouri, USA

Received 11 May 2017; revised 10 July 2017; accepted 16 August 2017
Published online 00 Month 2017 in Wiley Online Library (wileyonlinelibrary.com). DOI: 10.1002/jbm.a.36189

Abstract: While silicon nitride (Si_3N_4) is an antimicrobial and osseointegrative orthopaedic biomaterial, the contribution of surface topography to these properties is unknown. Using a methicillin-resistant strain of *Staphylococcus aureus* (MRSA), this study evaluated Si_3N_4 implants *in vitro* utilizing scanning electron microscopy (SEM) with colony forming unit (CFU) assays, and later in an established *in vivo* murine tibia model of implant-associated osteomyelitis. *In vitro*, the "as-fired" Si_3N_4 implants displayed significant reductions in adherent bacteria versus machined Si_3N_4 (2.6×10^4 vs. 8.7×10^4 CFU, respectively; $p < 0.0002$). Moreover, SEM imaging demonstrated that MRSA cannot directly adhere to native as-fired Si_3N_4. Subsequently, a cross-sectional study was completed in which sterile or MRSA contaminated as-fired and machined Si_3N_4 implants were inserted into the tibiae of 8-week old female Balb/c mice, and harvested on day 1, 3, 5, 7, 10, or 14 post-operatively for SEM. The findings demonstrated that the antimicrobial activity of the as-fired implants resulted from macrophage clearance of the bacteria during biofilm formation on day 1, followed by osseointegration through the apparent recruitment of mesenchymal stem cells on days 3–5, which differentiated into osteoblasts on days 7–14. In contrast, the antimicrobial behavior of the machined Si_3N_4 was due to repulsion of the bacteria, a phenomenon that also limited osteogenesis, as host cells were also unable to adhere to the machined surface. Taken together, these results suggest that the *in vivo* biological behavior of Si_3N_4 orthopaedic implants is driven by critical features of their surface nanotopography.

Key Words: silicon nitride, *Staphylococcus aureus*, antimicrobial, osseointegrative, electron microscopy

How to cite this article: Ishikawa M, de Mesy Bentley KL, McEntire BJ, Bal BS, Schwarz EM, Xie C. 2017. Surface topography of silicon nitride affects antimicrobial and osseointegrative properties of tibial implants in a murine model. J Biomed Mater Res Part A 2017:00A:000–#000.

INTRODUCTION

Staphylococcus aureus is responsible for the majority of chronic osteomyelitis cases; and these bone infections remain a major challenge in orthopaedics.[1] Additionally, these infections are considered to be incurable due to biofilm dwelling bacteria that persist within *Staphylococcus* abscess communities[2,3] (SACs or Brodie's abscesses[4,5]) and deep within cortical bone;[6,7] and costing billions of dollars each year.[8] Of particular concern is the community-associated methicillin-resistant *S. aureus* (MRSA) strain USA300 LAC, which now accounts for the majority of orthopaedic infections.[9] To address this concern, silicon nitride (Si_3N_4) has emerged as an orthopaedic implant material with remarkable antimicrobial potential compared to standard clinical implants made of stainless steel (SS), poly(aryl-ether-ether-ketone) (PEEK), and titanium (Ti). In a recent time-course study, Webster et al. demonstrated in a Wistar rat *Staphylococcus epidermidis* infection model that new bone formation around aseptically implanted Si_3N_4 (i.e., within the surgical area) was approximately 69% at 90-days post-operatively, compared with 24 and 36% for sterile PEEK and Ti implants, respectively.[10] In a parallel septic implantation arm of their study, new bone formation for Si_3N_4, Ti, and PEEK was 41, 26, and 21%, respectively, at this same time point. Most importantly, live bacteria were identified around PEEK (88%) and Ti (21%) implants, whereas none were present adjacent to Si_3N_4. The Si_3N_4 test samples used in the study by Webster et al. were

Correspondence to: E. M. Schwarz; e-mail: Edward_Schwarz@URMC.Rochester.edu
Contract grant sponsor: Amedica Corporation and National Institutes of Health; contract grant number: P30 AR069655

identical in composition and processing to the present study. They only differed in geometry and surface finish. Furthermore, chemical, sessile-wetting, electrokinetic, microstructural, and surface roughness analyses of these same materials have been performed previously by a number of researchers.[10–14] Interested readers are referred to these earlier studies for comparative details.

Another critical biomaterial property of orthopaedic implants is their compatibility within the bone microenvironment to allow for mesenchymal stem cell (MSC) adherence, differentiation, activation of bone forming osteoblasts, and overall osseointegration into the host bone.[11] In this regard, Si_3N_4 implants have also been shown to have remarkable advantages for orthopaedic applications, as quantitative assessment of osseointegration measured by resistance to implant push-out at 3-months post-implantation in a rat model demonstrated statistically superior bone growth and attachment compared with Ti and PEEK.[10] However, while empirical antimicrobial and osseosintegrative biomaterial properties of Si_3N_4 implants have been established,[12] the contribution of surface topography to these properties remained unknown. Therefore, this study was designed to evaluate *S. aureus* biofilm formation on two forms of Si_3N_4 standard implants (as-fired and machined) versus SS, Ti, and PEEK implants *in vitro*. We also performed descriptive scanning electron microscopy (SEM) studies of the behaviors of MRSA, macrophages, MSCs, and osteoblasts on the surface of as-fired versus machined Si_3N_4 implants using an established murine model of implant-associated osteomyelitis,[15] to test the hypothesis that surface topography of Si_3N_4 implants contributes to their antimicrobial and osseointegrative properties *in vitro* and *in vivo*.

MATERIALS AND METHODS

L-shaped murine implant fabrication

Flat wire (cross-section 0.2 × 0.5 mm^2; MicroDyne Technologies, Plainville, CT) was used to generate L-shaped SS and Ti implants as previously described.[15] The wire was cut to a 4 mm length, and bent into an L-shaped implant: long side 3 mm, short side 1 mm. Similarly, L-shaped PEEK and Si_3N_4 implants were fabricated by Amedica Corporation (Salt Lake City, UT). PEEK stock (PEEK Optima®, ASTM F2026-16, Invibio®, West Conshohocken, PA) was machined into the L-shaped implants using computer numerical controlled machining equipment (Haas Office Mill, Haas Automation, Oxnard, CA). Two groups of Si_3N_4 L-shaped implants were also produced through conventional ceramic fabrication techniques. They differed only in their surface morphology and final heat-treatment. Both groups were prepared by mixing and spray-drying Si_3N_4 powder (Ube SN-E10, Ube City, Japan), yttrium oxide (Y_2O_3, Grade C, H. C. Starck, Munich, Germany) and aluminum oxide, (Al_2O_3, SA8-DBM, Baikowski/Malakoff, Charlotte, NC) at percentages of 90.0, 6.0, and 4.0 wt %, respectively, along with appropriate binders and pressing aids. The resulting powder was pressed into rectangular blocks through uniaxial compacting equipment (TPA 30, Dorst America, Bethlehem, PA) at pressures in excess of 200 MPa. The specimens' features were then machined (Haas Office Mill) in their pressed state to shrink to either final- or near-final-size during subsequent densification heat-treatments. Samples were fired at a temperature in excess of 1700°C in a N_2 environment (CVI Belt and Batch Furnaces, Centorr-Vacuum Industries, Nashua, NH) to obtain closed-porosity, and further densified using hot-isostatic pressing (QIH 21, Avure Autoclave Systems, Columbus, OH) at a temperature exceeding 1650°C and N_2 gas pressures of >200 MPa. After densification, one group required no further processing and was designated as-fired. The morphology of this group of implants consisted of fine nano- to micron-size anisotropic prismatic ß-Si_3N_4 grains which projected from the surface of each implant [Fig. 1(A)]. The second group of Si_3N_4 implants was ground flat using a 120 grit diamond wheel on a surface grinder (Okamoto 12–24D Grind-X, Vernon Hills IL). The surface grinding operation removed the protruding grains from the surface, leaving only ground features [Fig. 1(B)]. After grinding, these implants were subjected to a N_2-annealing heat-treatment at 1400°C for 30 min.

MRSA inoculation of implants

Static cultures of a MRSA (USA300 LAC)[16] were obtained through overnight culture (outer diameter [O.D.] = 0.7 at 630 nm) of the bacteria in 10 mL of tryptic soy broth (TSB) media at 37°C,[17] which was used to contaminate the L-shaped implants ($n = 4$) as previously described.[15] Based on established protocols known to contaminate SS pins with 10^5 colony forming unit (CFU) of planktonic *S. aureus*,[15,18] implants were incubated in the MRSA culture for 20 min at room temperature, and then air dried for 5 min. To determine the inoculum, implants were placed into Eppendorf tubes with 1 mL of sterile saline and vortexed for 2 min, then 10-fold dilutions were plated on tryptic soy agar (TSA) to quantify CFUs after 24 h incubation at 37°C. To assess differences between the numbers of adherent MRSA on SS, Ti, PEEK, and Si_3N_4 (as-fired and machined) surfaces following *in vitro* exposure, two independent experiments with the five different implants ($n = 4$) were evaluated by CFU assay.

Statistical analysis

The results from the *in vitro* CFU assay studies were analyzed to determine significant differences versus as-fired Si_3N_4. The mean ± standard deviation (SD) CFU from each group ($n = 4$) was calculated, and significant differences were determined through one-way analysis of variance (ANOVA) in which $p < 0.05$ was considered significant.

Scanning electron microscopy

SEM was performed as previously described.[15] The implants from the *in vitro* studies were placed into 24 well plates, fixed in 2.5% glutaraldehyde/4% paraformaldehyde in 0.1*M* cacodylate overnight, and post-fixed in buffered 1% osmium tetroxide. A pipet tip was placed against the wall of the wells for fluid exchange or removal to reduce disruption of biofilm during dehydration in a graded series of ethanol to 100%. The pins were then critically point dried, mounted

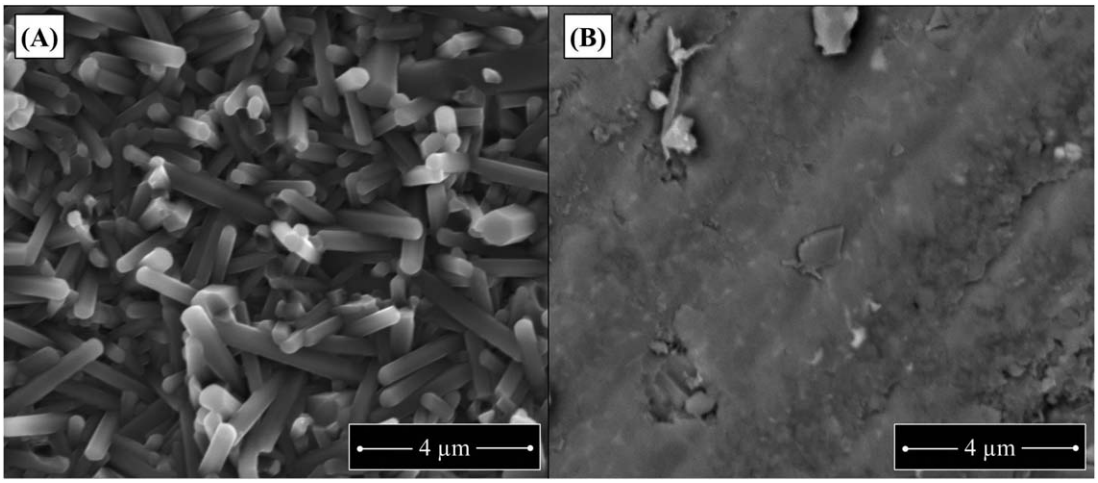

FIGURE 1. Topographical differences of native as fired and machined Si_3N_4 implant surfaces. Si_3N_4 as-fired and machined implants were fabricated and directly imaged by SEM as described in methods. Representative SEM images of these starting materials are shown to illustrate the fine nano- to micron-size anisotropic prismatic ß-Si_3N_4 grains projecting from the as-fired surface (A), versus the smooth annealed surface of machined Si_3N_4 (B).

onto aluminum stubs and sputter coated with gold prior to imaging using a Zeiss Auriga Field Emission SEM. Three SEM micrographs per sample group were randomly chosen for descriptive analysis.

In vivo studies

All *in vivo* experiments were performed following protocols approved by the University of Rochester Committee on Animal Resources. After sterilization and incubation in sterile saline or in an overnight culture of USA300 LAC, the air-dried L-shaped implants were surgically introduced into 8-week-old female Balb/c mice (Jackson Lab, Bar Harbor, ME). The surgical approach to press-fit the L-shaped trans-tibial implants from the medial to the lateral side was performed as previously described.[15] For cross-sectional *ex vivo* implant surface analysis, mice ($n = 3$) were euthanized on day 1, 3, 5, 7, 10, or 14. The tibiae were surgically removed with the implant intact, and fixed in 2.5% glutaraldehyde and 4% paraformaldehyde in 0.1*M* sodium cacodylate buffer overnight then decalcified in 14% ethylenediaminetetracetic acid (EDTA) for 3–4 days to facilitate removal of the implant and reduce the risk of damage to the biofilm. An incision into the bone facilitated the lifting out (perpendicular to the tibia) so any soft tissue adhering to the topside (the side to be evaluated by SEM) of the implant was retained intact. The implants were transferred to 24 well plates into phosphate buffered saline (PBS) for SEM processing as described above.

RESULTS

Differential responses of as-fired versus machined Si_3N_4 implants to MRSA exposure *in vitro*

To directly evaluate the antimicrobial surfaces of Si_3N_4 implants versus SS, Ti, and PEEK, SEM analyses were immediately conducted on the implants after *in vitro* exposure to MRSA. The results showed that large numbers of bacteria adhered to Ti and PEEK, with fewer numbers on SS and machined Si_3N_4 implants [Fig. 2(A–J)]. Remarkably, no bacteria were observed on native as-fired Si_3N_4 implant surfaces [Fig. 2(I)]. However, a closer inspection of the Si_3N_4 implants revealed bacteria bound to foreign material and culture debris on as-fired surfaces [Fig. 2(K–N)], and preferential bacterial adhesion to the flatter surfaces of the incompletely machined implants [Fig. 2(O–R)]. Collectively, these findings suggest that MRSA cannot directly adhere to native as-fired Si_3N_4 implant surfaces despite the opportunities afforded by the expanded surface area and crevices where 1 μm diameter cocci could reside. Moreover, these antimicrobial properties are largely due to surface topography, as they are lost by machining the surface.

To validate the descriptive SEM findings, CFUs on the surface of the implants were quantified following *in vitro* exposure to the overnight culture of MRSA (Fig. 3). The results demonstrated a significant 1.78-, 4.43-, and 2.84-fold reduction in CFU on as-fired Si_3N_4 implants versus SS, Ti, and PEEK, respectively ($p < 0.001$). Additionally, similar numbers of CFUs were recovered from machined Si_3N_4 versus SS, Ti, and PEEK implants, while a significant 3.3-fold reduction in CFU on as-fired versus machined Si_3N_4 implants was observed ($p = 0.0019$). Taken together, these *in vitro* exposure findings demonstrate the critical importance of surface topography for the inherent antimicrobial properties of as-fired Si_3N_4 implants, as MRSA cannot adhere directly to its native surface, but can adhere with similar affinity as it does on SS, Ti, and PEEK implants when its native surface is machined and nitrogen annealed.

Differential host responses to sterile and septic as-fired versus machined Si_3N_4 implants *in vivo*

To assess the effects of surface topography on Si_3N_4 implants *in vivo*, an established murine tibia model was utilized.[15] Initially, a cross-sectional time course evaluation was performed using sterile as-fired versus machined Si_3N_4 implants harvested from mice on days 1, 3, 5, 7, 10, and 14

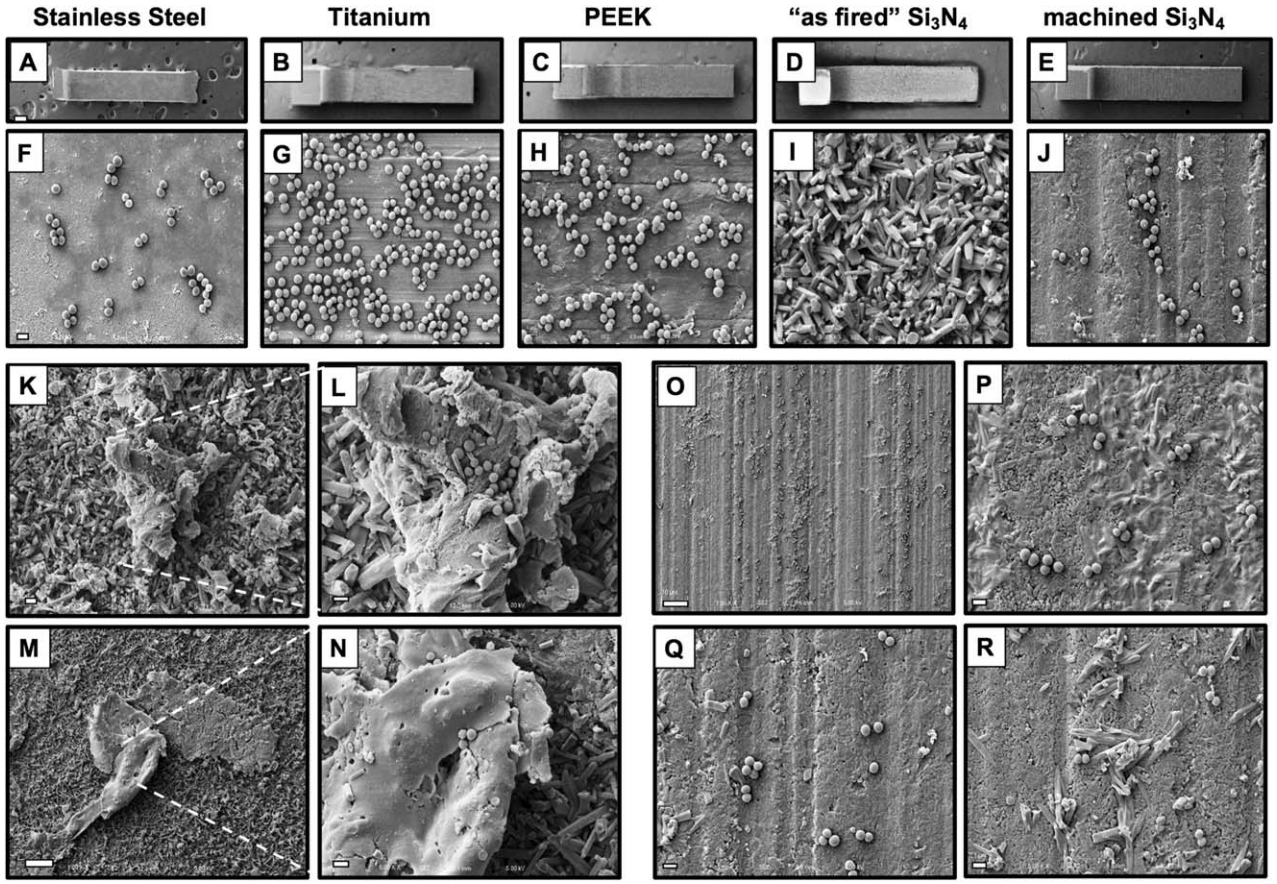

FIGURE 2. Native as-fired Si_3N_4 implant surfaces are highly resistant to MRSA adherence *in vitro*. SS, Ti, PEEK, as-fired Si_3N_4 and machined Si_3N_4 implants ($n = 4$) were submerged in an overnight culture (O.D. = 0.7 at 630 nm) of USA300LAC, air dried, and processed for SEM imaging. Representative low magnification images of the L-shaped implants are shown at ×30 ([A–E]; scale bar in A = 200 μm), and higher magnification images of regions containing adherent MRSA are shown at ×5000 ([F–J]; scale bar in F = 1 μm). We failed to identify bacteria that were directly adhering to native as-fired Si_3N_4 implant surfaces (I). However, bacteria were only observed on foreign material and culture debris (TSB precipitate and lysed bacteria) that adhered to the as-fired Si_3N_4 implant surfaces ([K] ×2000; scale bar = 5 μm; inset image [L] ×5000 scale bar = 1 μm) and ([M] ×1000; scale bar = 10 μm; inset image [N] ×5000 scale bar = 1 μm). In contrast, bacteria were readily found on machined Si_3N_4 implant surfaces ([O] ×1000 scale bar = 10 μm). High magnification images of nonuniformly machined areas demonstrated preferential bacterial adhesion to the flatter surfaces, and lack of bacterial adhesion to incompletely machined surface structures ([P–R] ×5000 scale bar = 1 μm).

after tibial insertion, through descriptive SEM (Fig. 4). The results demonstrated that the highly reactive as-fired Si_3N_4 implant surface progressively transformed toward osseointegration over time. Phenotypically, as-fired Si_3N_4 implant surfaces were highly reactive with host factors and blood cells shortly after implantation, as evidenced by the rich fibrin coating and presence of leukocytes and erythrocytes attached to this matrix [Fig. 4(B,B^1)]. By day 3 rounded/oval cells morphologically consistent with MSCs, were present on the surface [Fig. 4(D,D^1)]. The prominent cells on the implant surface on day 5 were rounded to polygonal in appearance, and were phenotypically consistent with differentiating MSCs [Fig. 4(F,F^1)]. Large polygonal mesenchymal cells consistent with an osteoblast phenotype first appeared on as-fired Si_3N_4 implant surfaces on day 7 [Fig. 4(N,N^1)], and thereafter these implants were primarily occupied by osteoblastic cells organizing to form a dense coating [Fig. 4(P,P^1,R,R^1)]. In contrast, machined Si_3N_4 implant surfaces were largely nonreactive with the host, and did not display any remarkable changes over time [Fig. 4(G–L,S–X)].

To assess the effects of surface topography on septic Si_3N_4 implants *in vivo*, the descriptive SEM cross-sectional time course study was repeated for as-fired versus machined Si_3N_4 implants that were exposed to a MRSA overnight culture prior to surgical implantation (Fig. 5). These results also showed that the highly reactive as-fired Si_3N_4 implant surface displayed a progressive transformation from a MRSA infected condition to an apparent preosseous interface over time. On day 1 post-operatively, bacterial biofilm on the implant surface appeared to be attacked by inflammatory cells [Fig. 5(B)], and the mature bacterial biofilm pods appeared elevated from the surface by inflammatory cells anchored with fibrin cables on day 3 [Fig. 5(D)]. On day 5, the eradicated bacteria appeared to be replaced by a mixture of round cells, which were morphologically consistent with macrophages, together with small numbers of polygonal cells [Fig. 5(F)]. Thereafter, the as-fired Si_3N_4 implant surface was covered with polarized cells with an osteoblastic appearance [Fig. 5(G–H)]. In contrast, machined Si_3N_4 implant surfaces were less

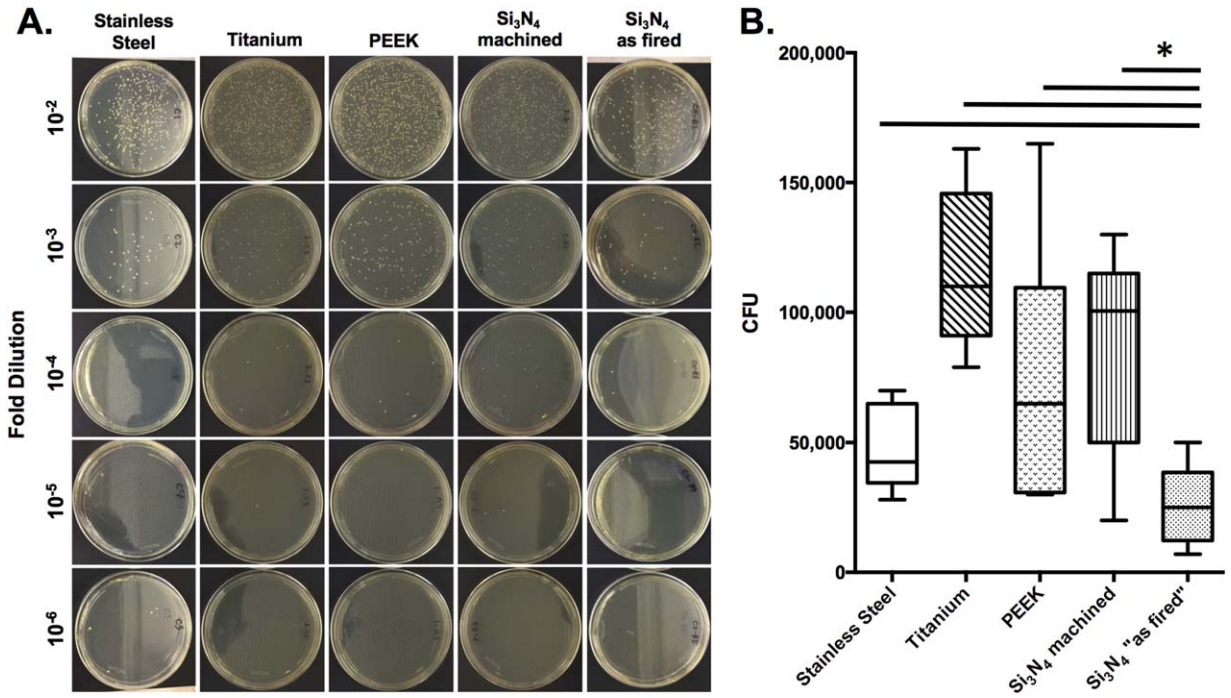

FIGURE 3. As-fired Si_3N_4 implants display reduced CFUs following exposure to MRSA *in vitro*. SS, Ti, PEEK, and Si_3N_4 implants ($n = 4$) were exposed to overnight cultures (O.D. = 0.7 at 630 nm) of USA300 as described in Figure 1. After air drying, the implants were added to 1 mL of sterile saline, vortexed, and serial dilutions were plated on TSA plates and incubated at 37°C for 24 h to determine CFUs. Data from one of the equivocal replicate experiments is presented. Representative examples to illustrate the CFUs on the dilution plates are shown (A), and the CFU data are presented as the mean ± SD ([B]; $*p < 0.002$ one-way ANOVA).

reactive with both bacteria and host cells. Bacteria were rarely found in biofilms on implants harvested 1-day postoperatively [Fig. 5(N)]. By day 3 no bacteria were found and few activated macrophages appeared on the surface [Fig. 5(P)]. Thereafter, machined Si_3N_4 implant surfaces were incompletely coated by red and white blood cells [Fig. 5(Q–X)].

DISCUSSION

Bone infections are the bane of orthopaedic surgery, of which the vast majority are caused by *Staphylococcal* species.[1] While the number of bone infections following primary elective surgery is low (1–5%), reinfection rates are very high (15–40%),[19–23] which has led to the orthopaedic paradigm that *S. aureus* infection of bone is incurable.[24] Additionally, surgical site infections are known to be a nonrandom event that is largely determined by patient-specific factors, as infections are caused by only a few prevalent nosocomial strains (i.e., MRSA USA300);[25] and implementation of the most rigorous surgical systems (i.e., Surgical Care Improvement Project measures) is incapable of reducing infection rates below 1%.[26,27] Moreover, approximately 13% of orthopaedic patients infected with *S. aureus* become septic and die from multiorgan failure.[28–30] Thus, there has been a tremendous quest to produce antimicrobial implants. In general, these efforts have been largely focused on coating existing orthopaedic implants with: (1) metal ions (e.g., silver[31] and copper[32]) which has proven to be limited due to toxicity issues;[33] and (2) antibiotics (e.g., gentamicin[34] and vancomycin[35]) which limits the osteoconduction of the implant. Thus, an important alternative approach is to find an implantable biomaterial that is inherently antimicrobial and osteoconductive.

Si_3N_4 is a synthetic nonoxide ceramic that is used in many industrial applications, and has been investigated or adapted as a biomedical material since 1989.[10,12,36–42] The rationale for using Si_3N_4-based implants in skeletal reconstruction is based on its favorable combination of mechanical strength, microstructure, and cytotoxicity.[12,41] Polished and porous implants made of Si_3N_4 have shown encouraging outcomes in spine and maxillofacial surgery.[12,41] Most interestingly, initial studies have demonstrated that Si_3N_4 is empirically antimicrobial and osteoconductive,[10] making it a very attractive biomaterial for orthopaedic surgery. In contrast to the limited clinical experience with Si_3N_4, implants made of SS, Ti, and their alloys have been used in skeletal reconstruction for many decades.[43,44] More recently, PEEK, a polymer with modest strength and a low modulus of elasticity compared with metal, has been investigated as an orthopedic biomaterial,[45] and is commonly used in spine surgery.[46] However, SS, Ti, and PEEK are not known to have inherent antimicrobial activities. Thus, this head-to-head study assessed the ability of MRSA to adhere to SS, Ti, PEEK, and Si_3N_4 implants *in vitro*. Additionally, as the role of surface topography in bacterial adherence to Si_3N_4 implants is unknown, as-fired versus machined Si_3N_4 implants were also compared. While the results of these *in vitro* experiments with MRSA (Figs. 2 and 3) corroborated

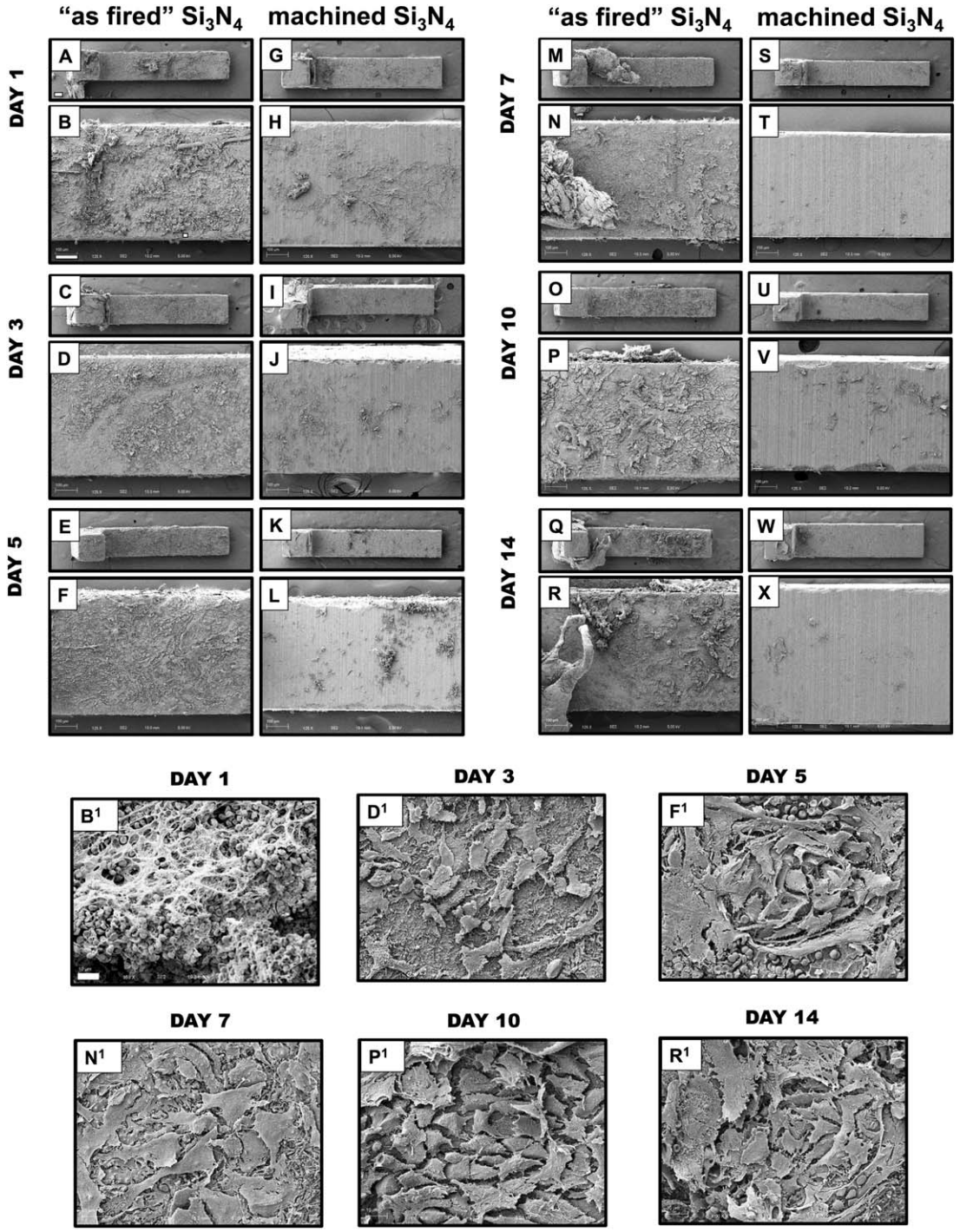

FIGURE 4. Differential host cell responses to sterile as-fired versus machined Si_3N_4 implants in bone over time. Sterile L-shaped as-fired and machined Si_3N_4 implants ($n = 5$) were surgically implanted into the tibiae of 6-week-old, female Balb/c mice, removed on the indicated day post-operatively, and processed for SEM (A–X). Representative low magnification images of the L-shaped implants are shown at ×30 (bar = 200 μm), and higher magnification images of regions containing host material are shown at ×125 (bar = 100 μm). Of note is the highly reactive as-fired Si_3N_4 implant surface, which displayed a progressive transformation toward osseous integration over time: day 1 white and red blood cells ([B,B^1] ×1000); day 3 rounded/oval cells (MSCs) ([D,D^1] ×1000); day 5 rounded to polygonal cells (differentiation MSCs) ([F,F^1] ×1000); day 7 large polygonal mesenchymal cells (osteoblasts) ([N,N^1] ×1000); days 10 and 14 osteoblastic cells organizing to form a dense coating ([P,P^1] ×1000 and [R,R^1] ×1000, respectively). In contrast, machined Si_3N_4 implant surfaces were largely nonreactive with the host, and did not display any remarkable changes over time.

prior studies demonstrating greater antimicrobial effects of Si_3N_4 implants compared to SS, Ti, and PEEK,[10,12] the more interesting observation was that MRSA cannot directly bind to the as-fired Si_3N_4 implant surface [Figs. 2(I,K–N)]. However, removal of the nanotopography through machining and nitrogen annealing rendered Si_3N_4 implants susceptible to MRSA adhesion [Figs. 2(J,O–R)]. It was also interesting to find that SS implants displayed greater antimicrobial activity

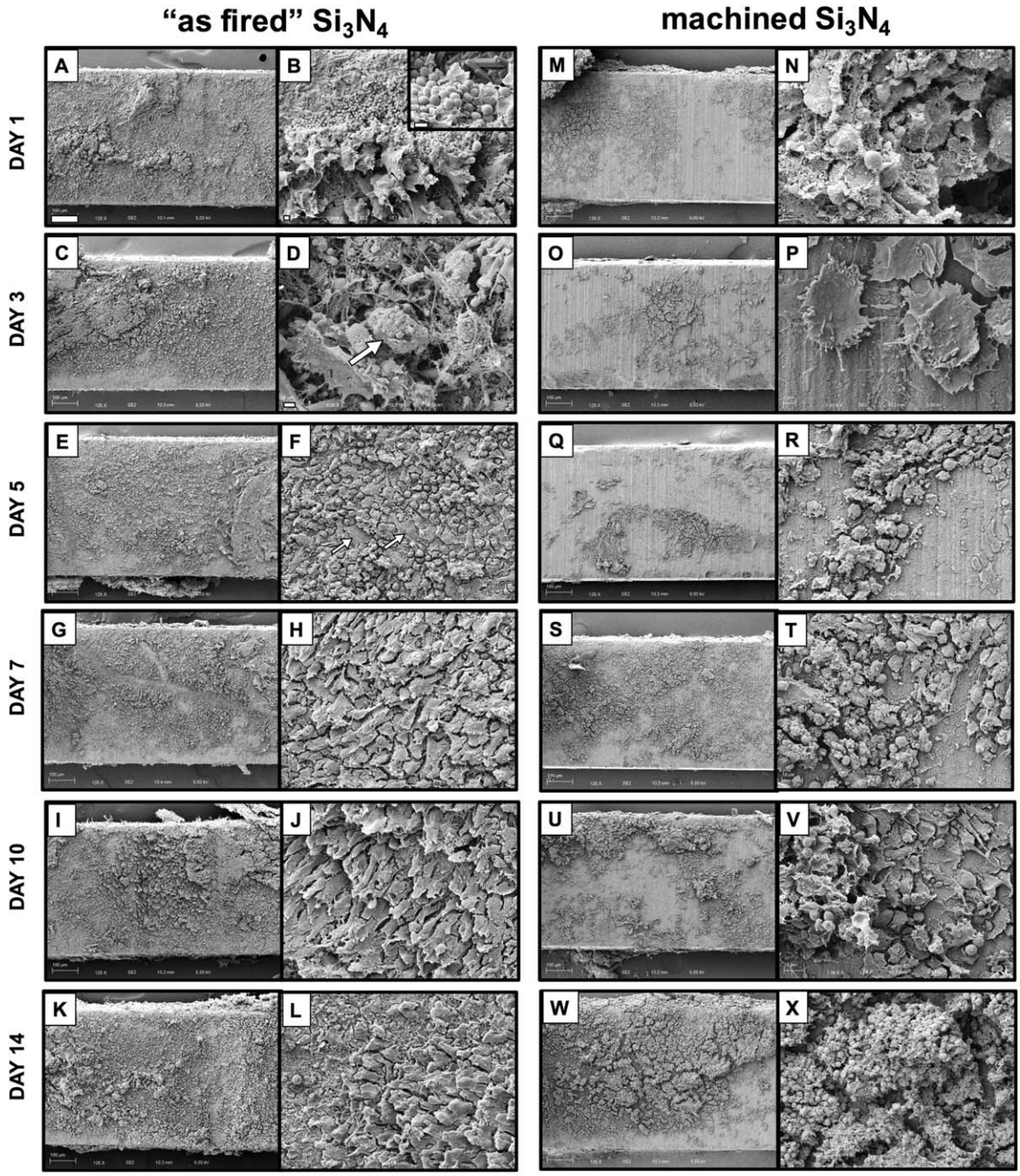

FIGURE 5. Differential host cell responses to MRSA contaminated as-fired versus machined Si_3N_4 implants in bone over time. Sterile L-shaped as-fired and machined Si_3N_4 implants ($n = 3$) were exposed to USA300LAC culture as described in Figure 1, surgically implanted into the tibiae of 6-week-old, female Balb/c mice, removed on the indicated day post-operatively, and processed for SEM (A–X). Representative ×125 images of the center of the L-shaped implants are shown (bar = 100 μm), and higher power images of regions containing host material are shown at ×1000 (bar = 100 μm). Of note is the highly reactive as-fired Si_3N_4 implant surface, which displayed a progressive transformation from a MRSA infected surface, to an osseous surface over time as follows: day 1 bacterial biofilm (inset image ×5000; bar = 1 μm) is attacked by inflammatory cells ([B]; ×2000 bar =2 μm); day 3 bacterial pod (arrow in [D]; ×5000; bar = 1 μm) is elevated from the surface by inflammatory cells anchored with fibrin cables; day 5 eradicated bacteria are replaced by mixture of round cells (macrophages) and the appearance of a few polygonal cells (arrows in [F]; ×1000; bar = 10 μm); days 7, 10, and 14 show polarized osteoblastic cells ([H,J,L] ×1000). In contrast, machined Si_3N_4 implant surfaces were less reactive with both bacteria and host cells as follows: day 1 bacteria are rarely found in biofilm ([N] ×5000; bar = 1 μm); day 3 no bacteria were found and few activated macrophages appeared on the surface ([P] ×3000; bar = 2 μm); days 5, 7, 10, and 14 display incomplete coating by red and white blood cells.

versus Ti implants, as assessed in our *in vitro* CFU assay (Fig. 3). As this finding is somewhat inconsistent with prior studies that have failed to observe similar findings,[47–49] follow-up experiments are warranted. While the present study did not delve into the mechanisms responsible for the observed differences, the enhanced resistance to MRSA by

the as-fired Si_3N_4 may be twofold. First, the acicular pillared nanostructured features of the as-fired surface inhibited initial attachment of MRSA cells. Second, there may be a chemical resistance associated with the minute elution of an oxidative form of nitrogen (i.e., peroxynitrite, $ONOO^-$). These combined mechanisms are plausible based on research from other investigators. For instance, Xu et al. demonstrated that a combination of nano-pillared polyurethane biomaterial (400–500 nm spikes) doped with a nitrogen emitting compound (*S*-nitroso-*N*-acetylpenicillamine) was more effective in inhibiting the bacterial adhesion of *S. epidermidis* than either treatment method alone;[50] and Pezzotti et al. specifically showed that the release of nitrogen from Si_3N_4 in the form of peroxynitrite was an effective deterrent in the attachment of *Porphyromonas gingivalis*.[51] Undoubtedly, the topography and higher surface area associated with as-fired in comparison to "machined" Si_3N_4 enhanced both mechanistic effects.

In order to best assess *in vivo* responses to as-fired and machined Si_3N_4 implants within the bone microenvironment, a murine tibia model designed to quantify biofilm formation within a prospective 1 mm^2 region of interest (ROI) was chosen.[15] It was surprising to discover that the murine host response to these Si_3N_4 implants was Boolean, as the vast majority of the as-fired surface was covered by day 1 post-operatively, while the machined surface remained naked throughout the 14 day study period (Fig. 4). Similarly, the analyzed ROIs of MRSA contaminated Si_3N_4 implants showed that the as-fired surfaces were dramatically more reactive with the host, rendering quantitative assessment of differences in the % surface coverage meaningless. Thus, while a notable weakness of these *in vivo* studies is the absence of quantitative analyses, the primary goal of identifying important differences between as-fired and machined Si_3N_4 surfaces was achieved. Moreover, the study provided important insights into the antimicrobial and osteoconductive mechanisms of this unique biomaterial. Specifically, several hypotheses were generated on observations that will serve as the scientific premise of future studies, including: (1) the inability of MRSA to directly adhere to native as-fired surfaces [Fig. 5(B,D)]; (2) the ability of host inflammatory cells and extracellular matrix fibers to elevate MRSA biofilm/pods from the as-fired surface to allow effective bacterial clearance by phagocytes [Fig. 5(A–F)]; and (3) the transformation from an inflammatory cell coated surface [Fig. 5(F)] to an osteoblastic coated surface [Fig. 5(E–L)]. On the negative side, observations demonstrating minimal host cell interactions with machined and nitrogen-annealed Si_3N_4 surfaces diminish enthusiasm for future studies with these types of implants.

In addition to the absence of quantitative outcome measures, there are three other notable limitations of this study. The first is that only USA300 was evaluated, rather than a multitude of methicillin sensitive and resistant strains of *S. aureus* that represent clinical infections. The decision to focus this exploratory study on USA300 was based on publications indicating that this MRSA strain is the most prevalent in surgical site infections,[9,25] and that different *S. aureus* strains behave similarly in the murine implant model.[15] It is also known that the presence of human serum/plasma can impact bacterial adhesion to implant surfaces.[52] Thus, appropriate follow-up studies are needed to confirm the clinical significance of our findings. The other limitation is the absence of formal radiographic, biomechanical, and histological analyses to assess osseointegration of as-fired versus machined Si_3N_4 implants. As these are critical factors that will determine the clinical utility of Si_3N_4 implants for various indications, future studies to establish differences and elucidate their osteoconductive mechanisms are warranted.

ACKNOWLEDGEMNTS

The authors wish to thank Gayle Schneider of the URMC Electron Microscope Shared Resource Laboratory for her technical assistance.

CONFLICTS OF INTEREST

B.J.M. is Chief Technology Officer of Amedica Corporation. He has received stock and is a paid employee. B.S.B. is Chairman of the Board, Chief Executive Officer, President and Principal Financial Officer of Amedica Corporation. He has received stock and financial compensation.

REFERENCES

1. Darouiche RO. Treatment of infections associated with surgical implants. N Engl J Med 2004;350:1422–1429.
2. Cheng AG, Kim HK, Burts ML, Krausz T, Schneewind O, Missiakas DM. Genetic requirements for *Staphylococcus aureus* abscess formation and persistence in host tissues. FASEB J 2009;23:3393–3404.
3. Cheng AG, McAdow M, Kim HK, Bae T, Missiakas DM, Schneewind O. Contribution of coagulases towards *Staphylococcus aureus* disease and protective immunity. PLoS Pathog 2010;6: e1001036.
4. Brodie BC. Pathological researches respecting the diseases of joints. J R Soc Med 1813;4:210–280.
5. Brodie BC. An account of some cases of chronic abscess of the tibia. J R Soc Med 1832;17:239–249.
6. Brady RA, Leid JG, Calhoun JH, Costerton JW, Shirtliff ME. Osteomyelitis and the role of biofilms in chronic infection. FEMS Immunol Med Microbiol 2008;52:13–22. Epub 2007/12/18.
7. de Mesy Bentley KL, Trombetta R, Nishitani K, Bello-Irizarry SN, Ninomiya M, Zhang L, Chung HL, McGrath JL, Daiss JL, Awad HA, Kates SL, Schwarz EM. Evidence of *Staphylococcus aureus* deformation, proliferation and migration in canaliculi of live cortical bone in murine models of osteomyelitis. J Bone Miner Res 2017;32:985–990.
8. Hernandez-Vaquero D, Fernandez-Fairen M, Torres A, Menzie AM, Fernandez-Carreira JM, Murcia-Mazon A, Guerado E, Merzthal L. Treatment of periprosthetic infections: an economic analysis. Sci World J 2013;2013:821650.
9. Kourbatova EV, Halvosa JS, King MD, Ray SM, White N, Blumberg HM. Emergence of community-associated methicillin-resistant *Staphylococcus aureus* USA 300 clone as a cause of health care-associated infections among patients with prosthetic joint infections. Am J Infect Control 2005;33:385–391.
10. Webster TJ, Patel AA, Rahaman MN, Sonny Bal B. Anti-infective and osteointegration properties of silicon nitride, poly(ether ether ketone), and titanium implants. Acta Biomater 2012;8:4447–4454.
11. Lewallen EA, Riester SM, Bonin CA, Kremers HM, Dudakovic A, Kakar S, Cohen RC, Westendorf JJ, Lewallen DG, Van Wijnen AJ. Biological strategies for improved osseointegration and osteoinduction of porous metal orthopedic implants. Tissue Eng Part B 2015;21:218–230.
12. Bal BS, Rahaman MN. Orthopedic applications of silicon nitride ceramics. Acta Biomater 2012;8:2889–2898.

13. Bock RM, McEntire BJ, Bal BS, Rahaman MN, Boffelli M, Pezzotti G. Surface modulation of silicon nitride ceramics for orthopaedic applications. Acta Biomater 2015;26:318–330.
14. Bock RM, Jones EN, Ray DA, Sonny Bal B, Pezzotti G, McEntire BJ. Bacteriostatic behavior of surface modulated silicon nitride in comparison to polyetheretherketone and titanium. J Biomed Mater Res A 2017;105:1521–1534.
15. Nishitani K, Sutipornpalangkul W, de Mesy Bentley KL, Varrone JJ, Bello-Irizarry SN, Ito H, Matsuda S, Kates SL, Daiss JL, Schwarz EM. Quantifying the natural history of biofilm formation in vivo during the establishment of chronic implant-associated *Staphylococcus aureus* osteomyelitis in mice to identify critical pathogen and host factors. J Orthop Res 2015;33:1311–1319.
16. Guo Y, Ramos RI, Cho JS, Donegan NP, Cheung AL, Miller LS. In vivo bioluminescence imaging to evaluate systemic and topical antibiotics against community-acquired methicillin-resistant *Staphylococcus aureus*-infected skin wounds in mice. Antimicrob Agents Chemother 2013;57:855–863.
17. Varrone JJ, de Mesy Bentley KL, Bello-Irizarry SN, Nishitani K, Mack S, Hunter JG, Kates SL, Daiss JL, Schwarz EM. Passive immunization with anti-glucosaminidase monoclonal antibodies protects mice from implant-associated osteomyelitis, inhibits biofilm formation, and mediates opsonophagocytosis of *Staphylococcus aureus* megaclusters. J Ortho Res 2014;32:1389–1396.
18. Li D, Gromov K, Seballe K, Puzas JE, O'Keefe RJ, Awad H, Drissi H, Schwarz EM. Quantitative mouse model of implant-associated osteomyelitis and the kinetics of microbial growth, osteolysis, and humoral immunity. J Orthop Res 2008;26:96–105.
19. Azzam K, McHale K, Austin M, Purtill JJ, Parvizi J. Outcome of a second two-stage reimplantation for periprosthetic knee infection. Clin Orthop Relat Res 2009;467:1706–1714. Epub 2009/02/19.
20. Ghanem E, Azzam K, Seeley M, Joshi A, Parvizi J. Staged revision for knee arthroplasty infection: what is the role of serologic tests before reimplantation? Clin Orthop Relat Res 2009;467:1699–1705. Epub 2009/02/26.
21. Parvizi J, Azzam K, Ghanem E, Austin MS, Rothman RH. Periprosthetic infection due to resistant staphylococci: serious problems on the horizon. Clin Orthop Relat Res 2009;467:1732–1739. Epub 2009/05/02.
22. Ferry T, Uçkay I, Vaudaux P, François P, Schrenzel J, Harbarth S, Laurent F, Bernard L, Vandenesch F, Etienne J, Hoffmeyer P, Lew D. Risk factors for treatment failure in orthopedic device-related methicillin-resistant *Staphylococcus aureus* infection. Eur J Clin Microbiol Infect Dis 2009;29:171–180. Epub 2009/12/01.
23. Salgado CD, Dash S, Cantey JR, Marculescu CE. Higher risk of failure of methicillin-resistant *Staphylococcus aureus* prosthetic joint infections. Clin Orthop Relat Res 2007;461:48–53.
24. Schwarz EM, Alt V, Kates SL. The 1st international consensus meeting on periprosthetic joint infection. J Orthop Res 2014; 32(Suppl 1):S1.
25. Limbago B, Fosheim GE, Schoonover V, Crane CE, Nadle J, Petit S, Heltzel D, Ray SM, Harrison LH, Lynfield R, Dumyati G, Townes JM, Schaffner W, Mu Y, Fridkin SK. Characterization of methicillin-resistant *Staphylococcus aureus* isolates collected in 2005 and 2006 from patients with invasive disease: a population-based analysis. J Clin Microbiol 2009;47:1344–1351.
26. Auerbach A. Healthcare quality measurement in orthopaedic surgery: current state of the art. Clin Orthop Relat Res 2009;467: 2542–2547.
27. Aslam S, Darouiche RO. Prosthetic joint infections. Curr Infect Dis Rep 2012;14:551–557.
28. van Hal SJ, Jensen SO, Vaska VL, Espedido BA, Paterson DL, Gosbell IB. Predictors of mortality in *Staphylococcus aureus* Bacteremia. Clin Microbiol Rev 2012;25:362–386.
29. Cram P, Lu X, Kates SL, Singh JA, Li Y, Wolf BR. Total knee arthroplasty volume, utilization, and outcomes among Medicare beneficiaries, 1991–2010. JAMA 2012;308:1227–1236.
30. Gedbjerg N, Larosa R, Hunter JG, Varrone JJ, Kates SL, Schwarz EM, Daiss JL. Anti-glucosaminidase IgG in sera as a biomarker of host immunity against *Staphylococcus aureus* in orthopaedic surgery patients. J Bone Joint Surg Am 2013;95:e1711–e1719.
31. Gosheger G, Hardes J, Ahrens H, Streitburger A, Buerger H, Erren M, Gunsel A, Kemper FH, Winkelmann W, von Eiff C. Silver-coated megaendoprostheses in a rabbit model–an analysis of the infection rate and toxicological side effects. Biomaterials 2004;25: 5547–5556.
32. Hoene A, Prinz C, Walschus U, Lucke S, Patrzyk M, Wilhelm L, Neumann HG, Schlosser M. In vivo evaluation of copper release and acute local tissue reactions after implantation of copper-coated titanium implants in rats. Biomed Mater 2013;8:035009.
33. Sansone V, Pagani D, Melato M. The effects on bone cells of metal ions released from orthopaedic implants. A review. Clin Cases Miner Bone Metab 2013;10:34–40.
34. Alt V, Bitschnau A, Osterling J, Sewing A, Meyer C, Kraus R, Meissner SA, Wenisch S, Domann E, Schnettler R. The effects of combined gentamicin-hydroxyapatite coating for cementless joint prostheses on the reduction of infection rates in a rabbit infection prophylaxis model. Biomaterials 2006;27:4627–4634.
35. Antoci V Jr, King SB, Jose B, Parvizi J, Zeiger AR, Wickstrom E, Freeman TA, Composto R, Ducheyne P, Shapiro IM, Hickok NJ, Adams CS. Vancomycin covalently bonded to titanium alloy prevents bacterial colonization. J Orthop Res 2007;25:858–866.
36. Howlett CR, McCartney E, Ching W. The effect of silicon nitride ceramic on rabbit skeletal cells and tissue. An in vitro and in vivo investigation. Clin Orthop Relat Res 1989;(244):293–304.
37. Kue R, Sohrabi A, Nagle D, Frondoza C, Hungerford D. Enhanced proliferation and osteocalcin production by human osteoblast-like MG63 cells on silicon nitride ceramic discs. Biomaterials 1999;20: 1195–1201.
38. Amaral M, Costa MA, Lopes MA, Silva RF, Santos JD, Fernandes MH. Si(3)N(4)-bioglass composites stimulate the proliferation of MG63 osteoblast-like cells and support the osteogenic differentiation of human bone marrow cells. Biomaterials 2002;23:4897–4906.
39. Amaral M, Lopes MA, Santos JD, Silva RF. Wettability and surface charge of Si3N4-bioglass composites in contact with simulated physiological liquids. Biomaterials 2002;23:4123–4129.
40. Amaral M, Lopes MA, Silva RF, Santos JD. Densification route and mechanical properties of Si3N4-bioglass biocomposites. Biomaterials 2002;23:857–862.
41. Neumann A, Unkel C, Werry C, Herborn CU, Maier HR, Ragoss C, Jahnke K. Prototype of a silicon nitride ceramic-based miniplate osteofixation system for the midface. Otolaryngol Head Neck Surg 2006;134:923–930.
42. Guedes e Silva CC, Konig B Jr, Carbonari MJ, Yoshimoto M, Allegrini S Jr, Bressiani JC. Tissue response around silicon nitride implants in rabbits. J Biomed Mater Res A 2008;84:337–343.
43. Dabrowski B, Swieszkowski W, Godlinski D, Kurzydlowski KJ. Highly porous titanium scaffolds for orthopaedic applications. J Biomed Mater Res B 2010;95:53–61.
44. Pohler OE. Unalloyed titanium for implants in bone surgery. Injury 2000;31(Suppl 4):7–13.
45. Kurtz SM, Devine JN. PEEK biomaterials in trauma, orthopedic, and spinal implants. Biomaterials 2007;28:4845–4869.
46. Toth JM, Wang M, Estes BT, Scifert JL, Seim HB 3rd, Turner AS. Polyetheretherketone as a biomaterial for spinal applications. Biomaterials 2006;27:324–334.
47. Rochford ET, Richards RG, Moriarty TF. Influence of material on the development of device-associated infections. Clin Microbiol Infect 2012;18:1162–1167.
48. Ribeiro M, Monteiro FJ, Ferraz MP. Infection of orthopedic implants with emphasis on bacterial adhesion process and techniques used in studying bacterial-material interactions. Biomaterial 2012;2:176–194.
49. Arens S, Schlegel U, Printzen G, Ziegler WJ, Perren SM, Hansis M. Influence of materials for fixation implants on local infection. An experimental study of steel versus titanium DCP in rabbits. J Bone Joint Surg Br 1996;78:647–651.
50. Xu LC, Wo Y, Meyerhoff ME, Siedlecki CA. Inhibition of bacterial adhesion and biofilm formation by dual functional textured and nitric oxide releasing surfaces. Acta Biomater 2017;51:53–65.
51. Pezzotti G, Bock RM, McEntire BJ, Jones E, Boffelli M, Zhu W, Baggio G, Boschetto F, Puppulin L, Adachi T, Yamamoto T, Kanamura N, Marunaka Y, Bal BS. Silicon nitride bioceramics induce chemically driven lysis in *Porphyromonas gingivalis*. Langmuir 2016;32:3024–3035.
52. Daeschel MA, McGuire J. Interrelationships between protein surface adsorption and bacterial adhesion. Biotechnol Genet Eng Rev 1998;15:413–438.